

Biorealistic Response in Optoelectrically-Driven Flexible Halide-Perovskite Single-Crystal Memristors

Ivan Matchenya,[†] Anton Khanas,[‡] Roman Podgornyi,[†] Daniil Shirkin,[†] Nikita Sizykh,[‡] Sergey Anoshkin,[†] Dmitry V. Krasnikov,[¶] Alexei Yulin,[†] Alexey Zhukov,[§] Albert G. Nasibulin,[¶] Ivan Scheblykin,^{||} Anatoly Pushkarev,^{*,†} Andrey Zenkevich,^{*,‡} and Alexandr Marunchenko^{*,†,||}

[†]*ITMO University, School of Physics and Engineering, St. Petersburg, 197101, Russian Federation*

[‡]*Moscow Institute of Physics and Technology (National research university), Institutskiy per. 9, Dolgoprudny, Moscow Region, 141701, Russia*

[¶]*Skolkovo Institute of Science and Technology, 30/1 Bolshoy Boulevard, 121205 Moscow, Russian Federation*

[§]*International Laboratory of Quantum Optoelectronics, HSE University, 190008, St. Petersburg, Russian Federation*

^{||}*Chemical Physics and NanoLund, Lund University, P.O. Box 124, 22100 Lund, Sweden*

E-mail: anatoly.pushkarev@metalab.ifmo.ru; zenkevich.av@mipt.ru;

a.marunchenko@metalab.ifmo.ru

Abstract

The transition to smart wearable and flexible optoelectronic devices communicating with each other and performing neuromorphic computing at the edge is a big goal in next-generation optoelectronics. These devices should perform their regular tasks supported by energy-efficient in-memory calculations. Here, we study the response of the CsPbBr₃ halide-perovskite single crystal fabricated on the flexible polymer substrate and integrated with the single-walled carbon nanotube thin film electrodes in a lateral geometry. We show both photodetection functions combined with the synaptic functionality in our device under the application of hybrid optoelectrical stimuli. Furthermore, we demonstrate that our device exhibits frequency-dependent bidirectional modification of synaptic weight with a sliding threshold similar to biologically plausible Bienenstock-Cooper-Munro learning. The demonstrated optoelectronic synaptic behavior in halide-perovskite single-crystals opens the opportunity for the development of hybrid organic-inorganic artificial visual systems.

Introduction

The modern computers based on Von Neumann architecture are saturating in terms of energy consumption to support the artificial intelligence (AI) algorithms and software that are coming into our daily life.^{1,2} Neuromorphic computing is an alternative computing paradigm inspired by the structure and operation of the human brain.³⁻⁵ The complexity of neurons and their connections is one of the prerequisites for the energy efficiency of biological organisms compared to classical computers with Von Neumann architecture.^{6,7,7-9} Within this framework, memristors defined simultaneously by several physical processes (state-variables) possessing the complexity of biological neurons and synapses can be considered as building blocks for neuromorphic computing hardware.^{7,8,10-13}

Decades of studying the biological brain have eventually led to novel efficient architectures of next-generation neuromorphic computers, particularly comprising memristive elements. In particular, the Bienenstock-Cooper-Munro (BCM) rule for synaptic modification has been developed to explain the response of the kitten and mice visual cortex neurons.¹⁴⁻¹⁷ In contrast to classical Hebbian learning, BCM requires bidirectional frequency-dependent synaptic weight modification with the tunable threshold.¹⁴ The memristive devices with this learning mechanism can be viewed as functional elements of the neural network hardware aimed at solving image recognition computing tasks.¹⁸⁻²⁰ However, the realization of the BCM learning rule in such systems requires at least the 2nd-order dynamics in memristive devices.^{14,19}

Furthermore, it would be advantageous to realize BCM learning on the memristive material platform having in addition a response to the light stimuli similar to that in the visual cortex neurons of biological organisms. In this way, the computing tasks related to image recognition (involving the light source) would be processed naturally "in-materia".^{21,22} In order to realize such approach, one has to find a material with intrinsically complex dynamics similar to neurons, which is controlled by at least two state variables, and in addition can be tuned by light.

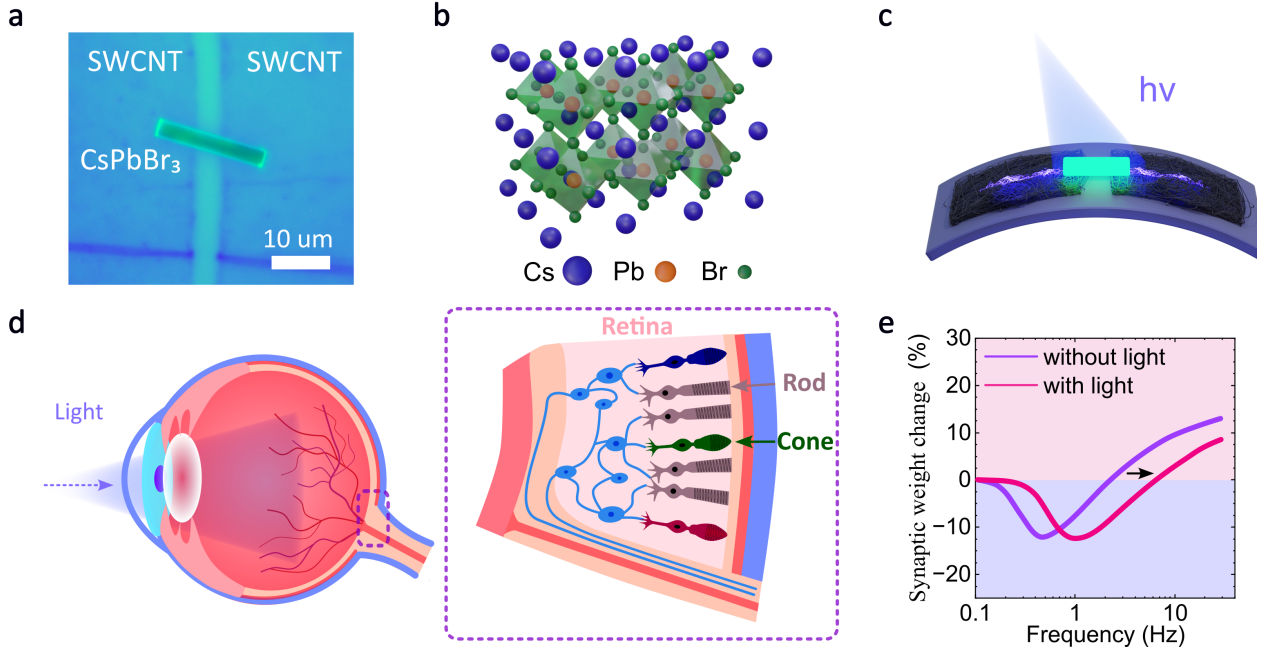


Figure 1: **Concept of making biologically plausible visual system based on CsPbBr₃ single-crystal.** (a) Microscopy image of a perovskite single crystal on the flexible substrate connected to SWCNT symmetrical electrodes (photoluminescent image of the real device). (b) The orthorhombic structure of the employed CsPbBr₃ single-crystal. (c) Operation of a single-crystal device under the application of optoelectrical stimuli combined with mechanical bending. (d) An eye transmits light towards the retina shell consisting of light-sensitive cones, sending a collective response signal to the brain. (e) An example of biological response under hybrid optoelectrical stimuli following the Biennstock-Cooper-Munro rule. The synaptic weight change is frequency-dependent showing the depression region at low frequencies followed by facilitation at high frequencies of internal input pulses. The sliding threshold (separating depression and facilitation) is affected by the light stimuli.

Halide-perovskite materials have been comprehensively studied aiming at optoelectronic applications such as photodetectors and solar cells,^{23–25} but recently also for memory applications^{26–28} due to their mixed-ionic conduction.^{19,29,30} Noticeably, the signature of the 2nd order dynamics combined with the BCM learning rule has been previously achieved by the group of Ielmini et al. where the triplet-spike-time-dependent plasticity scheme was used.²⁶

In this work, we study the response of cesium lead tribromide halide-perovskite (CsPbBr₃) single-crystals. The microcrystals electrically connected to the single-walled carbon nanotube (SWCNT) thin film electrodes are placed on the flexible substrates, thus imitating the cones embedded in the flexible human retina (Fig.1). We demonstrate the synaptic functionalities

of our devices such as paired-pulse facilitation, paired-pulse depression, and spike-rate dependent plasticity. We further show both frequency-dependent potentiation and depression in the dark and in the presence of light illumination similar to the biorealistic Bienenstock-Cooper-Munro learning behaviour. We explain such behavior upon hybrid optoelectronic stimuli by the competition of the capacitive- and inductive-like features coexisting in the charge carrier dynamics of halide perovskite semiconductors.

Results and discussion

Firstly, emphasize that we choose the lateral metal-semiconductor-metal type of the optoelectronic device.^{23,29} In such geometry, we are able to directly probe the dynamics of halide-perovskite semiconductors as compared to the typical vertical device structure with additional charge transport layers. To enable such structure, we use a chemically inert single-wall carbon nanotube (SWCNT) thin film as an electrode material and cesium-lead tribromide (CsPbBr_3) orthorhombic perovskite single-crystal as the semiconducting functional material (Fig.1a-c) similar to our previous works.^{23,29} While assembled on the flexible substrate, our crystals can be envisioned as artificial cones embedded in the eye retina (Fig. 1d). The additional advantage of halide-perovskite single crystals is their superior charge transport properties over the polycrystalline samples,^{23,31-34} as confirmed by the development of large-scale integration technologies in optoelectronic vision applications.³⁵⁻³⁸ Therefore, the possibility to feature BCM-like dynamics (Fig. 1e) in the single-crystal-based systems would provide additional benefits for neuromorphic computing by integrating existing optoelectronic solutions while developing hybrid optoelectronic architectures.

The fabrication of the CsPbBr_3 single-crystal memristor consists of the following stages. Firstly, the single-wall carbon nanotube (SWCNT) thin film is dry-transferred³⁹ on the flexible polyethylene naphthalate material (PEN) substrate (Fig.2a) Then, the SWCNT film is sliced into two separate electrodes (Fig.2b) using femtosecond laser ablation²³ (for details,

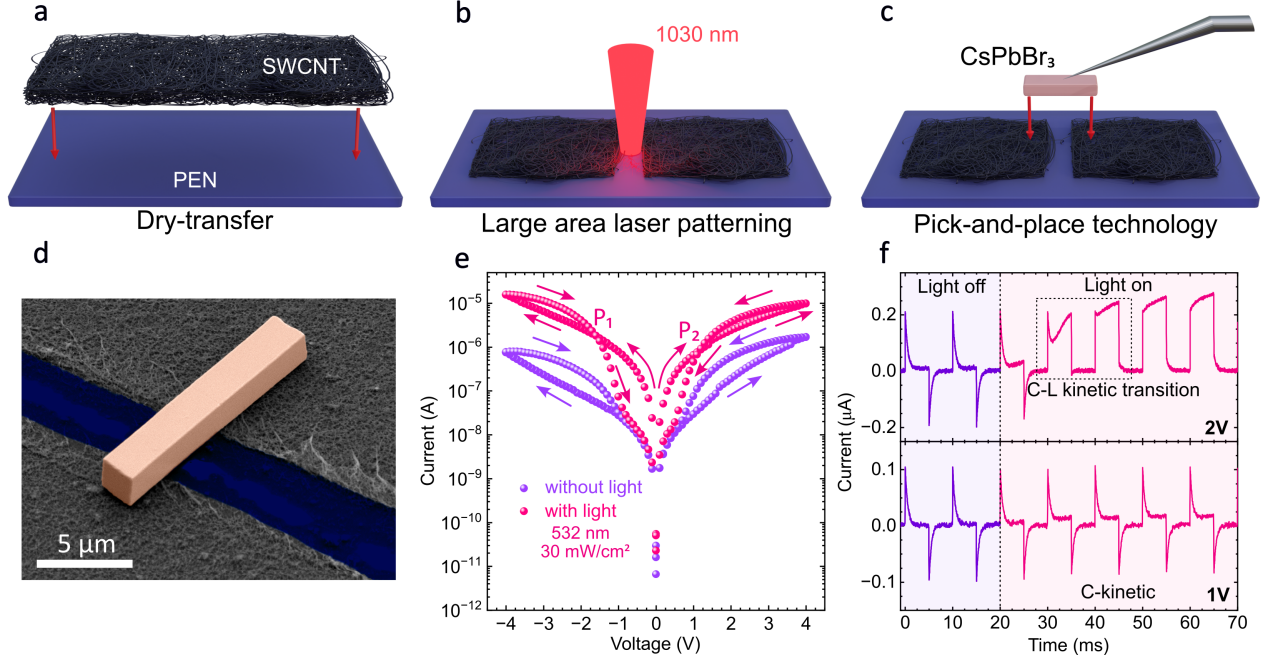


Figure 2: **The fabrication and optoelectronic operation of CsPbBr₃ single crystal.** (a) Dry-transfer deposition of SWCNT on the flexible PEN substrate. (b) Femtosecond laser cutting of SWCNT thin film into two symmetrical electrodes. (c) Dry transfer of CsPbBr₃ single crystal on the top of SWCNT thin film electrodes. (d) SEM image of the as-fabricated device. (e) Current-voltage curve, in dark (purple curve) and under illumination (pink curve). The P_1 and P_2 are points where the hysteresis type changes from regular to the inverted. Arrows indicate the voltage sweeping order. (f) The optoelectronic transient response of the CsPbBr₃ single-crystal. The plot is split into the regimes without illumination and with illumination. At a low bias (1 V) the response is capacitive-dominant, while at a higher (2 V) bias the transition from a capacitive-like response to an inductive-like response is visualized.

see the Methods section). Afterward, we perform solution-processed synthesis of (CsPbBr₃) single-crystals⁴⁰ and implement their further dry transfer (Fig.2c) on top of as-prepared SWCNT film electrodes (for details see Methods).

As a result, we obtain lateral MSM type of structure SWCNT-CsPbBr₃-SWCNT (Fig.2d), forming symmetrical Schottky contacts with the same Fermi levels of the used components.^{41,42} The interelectrode distance of about 5 μm (FIG.2d) is comparable with the charge carriers diffusion length^{43–45} of the halide-perovskite semiconductors which is desirable for efficient charge carrier extraction and subsequent efficiency of the device. To validate the stability of the formed contact between SWCNT and CsPbBr₃, we applied optoelectrical

stimuli to the device and measured the response for each of 5000 bending cycles. As a result after 20 000 bending cycles, the device response decreased to 85 % of its initial value (FIG.S1, Supplementary Information), thus signifying the stable electrical contact.

Current-voltage measurements on the device in the dark and under continuous wave (CW) light illumination of 30 mW/cm² at 532 nm wavelength are shown in Fig. 2e (see also FIG.S2, Supplementary Information; for a detailed description of the optoelectrical setup, see Methods). The hysteresis $I - V$ curves in the dark have an inverted inductive-like response, where the current on the forward scan is higher than that of the reverse scan.⁴⁶ Such a response in our structure can be attributed to the modulated Schottky contacts by intrinsic halide-perovskite mobile ions.^{27,29,47,48} By contrast, under light illumination the hysteresis becomes more complex (Fig. 2e). At low voltages it is capacitive-like, while at high voltages it becomes inductive-like. The transition between these two regimes is indicated on the plot as P₁, P₂ points (around -1.6 V and 1.2 V respectively). We note that this type of complex hysteresis under illumination is commonly observed in halide-perovskite optoelectronic devices with various structures.⁴⁹⁻⁵⁴ The explanation of such hysteresis transition in Fig. 1e was given by the Juan Bisquert group^{52,54} and is attributed to the coexistence of inductive and capacitive-types of response in perovskite devices.^{49,55}

Since the current-voltage measurements are a complex technique that implies the scanning of the voltage, it is possible to track the evolution of optoelectronic response by applying the periodic pulses of the same voltage amplitude. In Fig. 2f we show the transient response of photocurrent passing through the crystal, under the applied bias of 1 V (2 V) and light intensity 30 mW/cm². It can be seen that the current absolute value increases and matches Fig. 2e. The initial slope upon application of 1V is attributed to the capacitance discharge (Fig. 2f). However, at 2 V, the inductive type of the response equilibrates after some time (Fig. 2f). This shows that the light activates different types of dynamic variables at the timescale of tens of milliseconds. Similar behavior has been recently observed in FTO/PEDOT/MAPbBr₃/Au device architecture and related to the phenomenon of pho-

toinduced chemical inductor.⁵⁵ Such transient kinetics shows that the combination of both voltage amplitude and light intensity defines the type of equilibrated photocurrent response (either capacitive or inductive) (see also FIG.S3, Supplementary Information). Therefore, our CsPbBr₃ MSM device contains at least two competing state variables (represented in competing electric circuit branches) under hybrid optoelectrical stimuli.

In neurobiology the time-dependent dynamics is related to the Ca^{2+} cation concentration, which controls the release of neurotransmitters and synaptic plasticity in biological synapses under different external stimuli.⁵⁶ Its dynamics can be tracked by paired pulse facilitation (PPF) - one of the characteristics of short-term plasticity. It is manifested by the change in the amplitude of the excitatory postsynaptic current (ESPC) under the second pulse from the pair governed by Ca^{2+} cations influx enhancement. By analogy, the dynamical response in our CsPbBr₃ single-crystal memristors is governed by mixed ionic-electronic conduction, where the intrinsic perovskite mobile ions play a role of Ca^{2+} cations, while the modulated Schottky contact^{19,29} that of a synaptic membrane potential.⁵⁷

In order to track the short-term plasticity functionality in our memristors, we applied the paired voltage pulses with 3 V with different mutual time interval (for details, see Methods). Importantly, taking into account the dynamical process at the time scale of tens of milliseconds (Fig. 2f), the interval between pairs pulses was selected so that the device returned to the initial state. The PPF index is the relative change in the current between the first and second pulses in a pair as a function of the interval between two pulses is illustrated in Fig.3a. In the case of the dark, the PPF index reaches the maximum value of about 250 %. After increasing the interval between the two pulses up to 60 ms, it decreases down to 2-5% (Fig.3a). By contrast, under persistent light illumination of 30 mW/cm², we surprisingly revealed a slight depression effect (Fig.3a).

To unveil the observed short-term plasticity dynamics, we used equivalent circuit formalism (Fig.3b, 3c). We consider two main parts of competing electrical circuit branches with either capacitive or inductive dynamics. The parallel connection between these branches

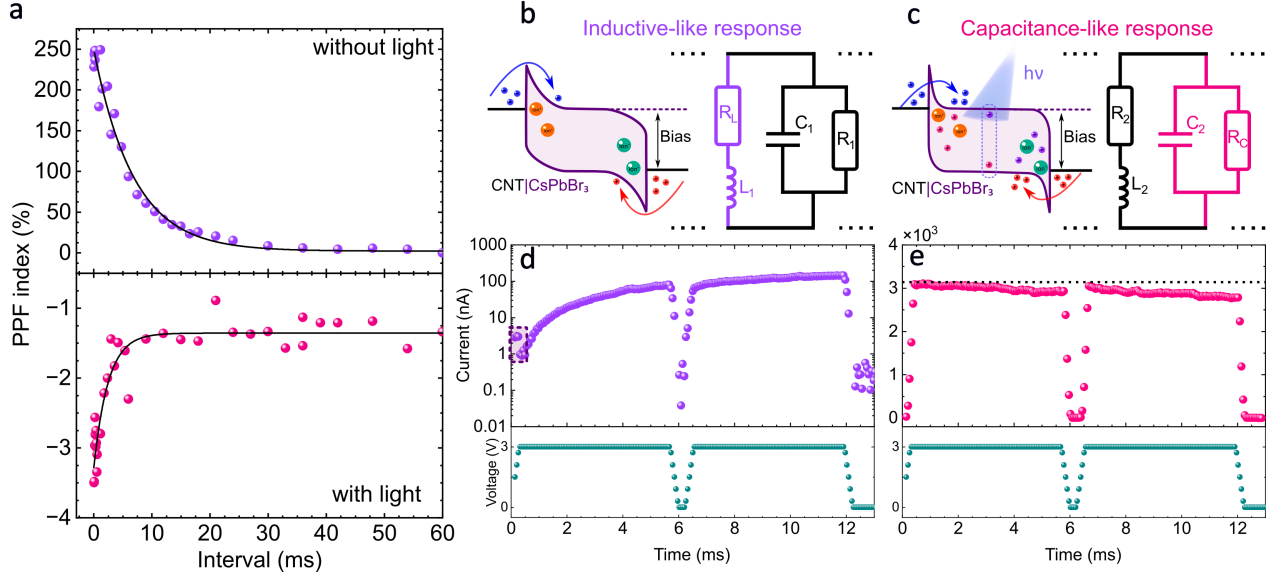


Figure 3: **Short-term plasticity of CsPbBr₃ single-crystal memristor under hybrid optoelectrical stimuli.** (a) Relative change in the EPSC, induced by paired pulses (3 V amplitude and 6 ms length) as a function of their mutual interval. Under dark conditions, the paired-pulse-facilitation type is present (purple curve), while under 30 mW/cm² illumination intensity, paired-pulse depression is observed (pink curve). (b,c) The schematic electronic band diagrams are the corresponding parts of the schematic electrical circuit equivalent scheme. Big red and green balls on the diagrams represent intrinsic perovskite mobile ions, coexisting together with injected electrons (blue) and holes (red), and with photogenerated electrons and holes in case of light illumination (d). In the dark, the inductive branch of the electrical circuit dominates, while under persistent illumination the capacitive one dominates. (c) Inductive-like response gives rise to the paired-pulse facilitation of single-crystal memristor in the dark. (d) Capacitive-like response supports paired-pulse depression of the single-crystal memristor under illumination. The green curve shows the profile of applied voltage pulses on (d,e) .

highlights the competition between the current dynamics which can flow through either of the circuit branches in parallel. We note here, however, that our intention is not to build the full equivalent circuit of CsPbBr₃ single-crystal memristor similarly to the other works on halide-perovskite devices.^{53,58} Such approach would additionally require more complex impedance spectroscopy measurements.^{59,60} Instead, our choice of these circuit branches is motivated by their frequent appearance and successful implementation in the literature covering halide-perovskite optoelectronic devices,^{46,49,52–54,58,61,62} and by their ability to qualitatively explain both inductive and capacitive types of the responses of our single-crystal

memristor (Fig.2e,f, Fig 3a,d,e).

A pair of pulses from the PPF experiment is shown in Fig. 3d (in dark) and in Fig. 3e (under illumination). The inductive circuit branch dominating our device in the dark case (Fig. 3d) originates from the tunable Schottky contact. Under the applied electric field, the mobile ions are driven toward the contact where they tune electrostatically the energy barrier for further bipolar injection of carriers (see electronic band diagram in Fig. 3b).^{29,63} The inductive response is naturally delayed in time. Initially, during the very first few milliseconds, the capacitive-type response can be seen (Fig. 3d). Such delayed inductive response (defined by the speed of barrier change) is governed by the slower dynamics of ionic carriers as compared to the electronic ones.^{53,58}

On the contrary, under laser illumination the dynamics is different. While the photocurrent level increased about 30 times compared to the dark case (Fig.3e), a clear signature of capacitive dynamics is observed. It is worth mentioning that to bring more contrast between the memristor response with and without light, we applied the light intensity 3 seconds prior to the start of electrical pulses. As a result, a clear change in the slope and timescale (from sub ms to tens of ms) of the capacitive charging was observed (Fig. 3e). This effect may originate from the light-enhanced capacitance. In fact, giant-light-induced capacitance has been demonstrated in halide-perovskite solar cells operating without external electrical field under similar light excitation conditions.^{59,64–66}

In order to demonstrate biorealistic response in our perovskite-based optoelectronic memristor, we investigated the experience-dependent postsynaptic behavior and response selectivity. For this, we performed spike-rate-dependent-plasticity (SRDP) measurements under hybrid optoelectronic stimuli Fig.4a,b (see Methods and FIG.S4, Supplementary Information). The 4 V pulses with the duration of 200 μ s were applied sequentially, consisting of 3 frequencies: low-intermediate-high (1kHz \rightarrow 2.5 kHz \rightarrow 4 kHz \rightarrow 2.5 kHz \rightarrow 1 kHz, respectively).

In the dark case, we observe the classical intermediate-high-intermediate transition lead-

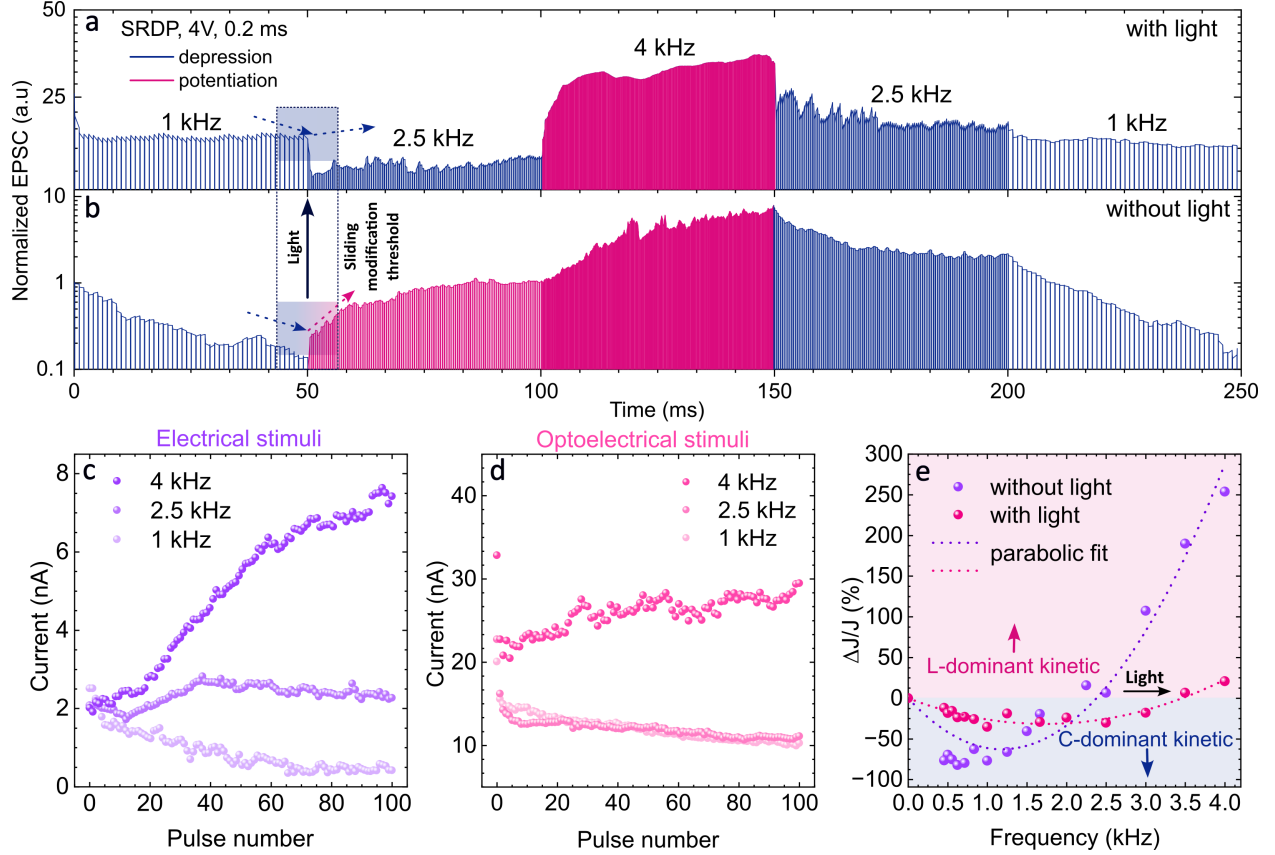


Figure 4: **Experience-dependent synaptic plasticity featuring bidirectional modification under hybrid optoelectrical stimuli.** (a-b) SRDP measurements with different pulse frequencies performed both under electrical a) and optoelectrical b) stimuli. (c-d) Current response to 100 consecutive pulses with different frequencies under electrical and optoelectrical stimuli, respectively. (d) The synaptic weight change inside a pulse train consisting of 100 pulses versus the frequency of pulses inside the pulse train shows the "tick-like" shape similar to the BCM theory. The plot is separated into two parts for positive and negative relative change of synaptic weight. The light intensity shifts curve minimum showing the sliding threshold property. The dotted line indicates parabolic fit.

ing to the increase (decrease) in synaptic weight at the higher (intermediate) frequency. This is a typical SRDP behavior that has been shown for a vast set of memristive material.^{13,19,67,68}

In addition, we see abnormal features like the decrease of synaptic weight while applying low pulse repetition frequency. This feature is similar to the capacitive memristor dynamics when applying transient pulses at the lower voltage (Fig. 2f). Therefore, it is possible to both decrease and increase the synaptic weight of our memristors in the dark, as anticipated for the BCM dynamics.¹⁴

Under light illumination the situation becomes more complex (Fig. 2a). The total synaptic weight increases following the light-absorbing property of our single-crystal (Fig. 2e, 2f,3e). At the low pulse repetition frequency (1 kHz) we were not able to see the capacitive dynamics, but after switching to the higher frequency, we observed an immediate (at the time scale of one or several pulses) decrease of synaptic weight. Therefore, under persistent light illumination we have identified the frequency range where the synaptic weight initially decreases, and later, normally, increases at a higher repetition frequency (Fig. 2a).

To support the aforementioned experiments, we applied pulse trains of 100 pulses with different pulse repetition rates (Fig. 4c, 4d) (for details see Methods). We clearly observe that by changing the frequency, we can both decrease the synaptic weight within a pulse train (in the case of low frequency) and increase the synaptic weight (in the case of high frequency). Notably, both cases are observed under dark and light illumination conditions, the frequency where synaptic modification within a pulse train changes its sign is higher in the case of illumination (Fig. 4c, 4d).

We then performed the frequency-dependent measurements of synaptic weight change within a pulse train of 100 pulses and fitted the experimental data with the parabolic fit (Fig. 4e). We note that both electrical and optoelectrical measurements have shown the increase and decrease of the current (Fig. 2f, Fig. 3d,e, Fig. S4 Supplementary Information), which can be related to the competing capacitive and inductive types of dynamics present in our memristors. The shape of the obtained curve is similar to the one predicted by the Bienenstock–Cooper–Munro (BCM) theory,^{18,69,70} with all of the main features present: bidirectional synaptic modification and sliding threshold which is emulated in our case by the change of parabola minimum in case of addition of optical stimuli.

Conclusions

To conclude, we have studied single-crystal CsPbBr₃ memristors assembled in the lateral geometry on a flexible substrate. They exhibit a photodetecting functionality with high responsivity combined with the stability to mechanical deformations. The short-term plasticity and experience-dependent plasticity measurements indicated the presence of both capacitive- and inductive-like dynamics. The coexistence of these dynamic processes at different time scales allows for the observation of the biological type of the response as anticipated by the BCM theory, where light intensity tunes the sliding threshold. Further extensive research is needed to quantitatively confirm the BCM learning in halide-perovskites driven by optoelectrical stimuli, supported by the wide range of optoelectrical stimuli excitation and as well theoretical modeling.

Our results demonstrate that halide-perovskite single-crystal devices hold promise for the development of a novel type of hybrid optoelectronic devices, combining simultaneously the functionalities of a photodetector and a memristor and in some cases electroluminescence,⁷¹ capable of processing information "in-memory" via both optical and electrical "channels". Finally, since halide-perovskites can be used as high-sensitivity photodetectors easily integrated on the flexible substrate and, furthermore, can exhibit the functionality of visual cortex neurons (following BCM dynamics), hybrid devices comprising halide perovskite as a functional material look an ideal candidate for the artificial biorealistic visual systems.

Methods

Synthesis of SWCNT

Thin films of single-walled carbon nanotubes (SWCNTs) were produced using an aerosol (floating catalyst) chemical vapor deposition (CVD) method⁷² followed by a simple filtration via a nitrocellulose membrane (HAWP, Merck Millipore). For the aerosol CVD, fer-

rocene (98%, Sigma Aldrich) was employed as a catalyst precursor while CO (99.99% Linde gas) acted as a carbon source. Ferrocene was transferred with a CO stream as a vapor to decompose upon reaching the hot zone (880 °C) of a quartz tube. The formation of Fe nanoparticles from ferrocene allows the catalytic Boudouard reaction ($2 \text{ CO} = \text{C} + \text{CO}_2$) to nucleate and produce nanotubes. Carbon dioxide (99.995% MGPZ) introduction tunes the nanotube properties (e.g., diameter distribution) and governs the process reactor productivity.⁷³ The collected films consisted of individual SWCNTs exhibiting a mean diameter of ca. 1.9 nm, high quality, and random spatial orientation. After the deposition, SWCNTs form a randomly oriented uniform film suitable for further dry-transfer⁷⁴ onto different types of a substrate.⁷⁵

Synthesis of CsPbBr₃ single crystals

To obtain CsPbBr₃ microcrystals we implement solution-processed synthesis by the protocol reported by Pushkarev et al.⁴⁰ Firstly, we prepare 0.1 M solution of metal halides (PbBr₂ and CsBr) in anhydrous dimethylsulfoxide (DMSO) in the N₂-filled glovebox. Afterwards, 2 μL of precursor ink was dropped on the nanostructured Al₂O₃ substrate (cleaned for 5 min, in water, and then, for 5 min in 2-propanol in an ultrasonic bath). Next, these substrates were placed in a Petri dish with 250 μL of 2-propanol and dried for 30 min at 70° C. As a result, a number of microcrystals on the target substrate were ready for further dry transfer.

Device fabrication

The as-prepared SWCNT films were dry-transferred on a polymer substrate (PEN). Then, 20 μl of isopropanol were dropped on SWCNT and evaporated at 70° for 5 minutes. Next, SWCNT thin film was cut by a femtosecond laser with a pulse duration of 270 fs at a wavelength of 1030 nm. The Laser beam was focused through 50x objective (NIR Mitutoyo, NA = 0.65), which gives the 3-5 μm interelectrode distance between the cut SWCNT slices. Afterward, we perform the dry transfer of the single crystals from the target substrate to

the interelectrode distance of the as-prepared SWCNT film electrode visualizing the whole process with the optical microscope.

Optoelectrical measurements

To perform combined optoelectrical measurements the sample was mounted on Cascade Microtech Summit 11000M probe station. The probes were landed on Pt layers, and deposited onto two separated Si substrates, which were connected with the SWCNT thin film electrodes via 50 μm golden wires and silver paste. Keysight B1500A semiconductor device analyzer was used for the electrical measurements. The optical stimuli were performed with the use of a CW 532 nm wavelength laser with an intensity of 30 mW/cm^2 . The current-voltage curves were measured using the source-measure unit (SMU) of the Keysight B1500A semiconductor device analyzer in the quasi-DC mode with the staircase sweeps with minimum integration time per voltage point of 2 μs .

Measurements of synaptic functionality

The pulsed measurements (paired-pulse facilitation/depression and spike rate-dependent plasticity) were performed using the Keysight B1530A waveform generator/fast measurement unit (WGFMU) module of the Keysight B1500A apparatus. The voltage pulses were generated and the current response was measured with two WGFMU modules with a best time resolution of 10 ns. To measure the PPF/PPD effect, we applied 20 pairs of pulses for each value of time interval between two pulses in the pair, averaged the current values I_1 and I_2 throughout the pulses, calculated PPF/PPD index as the relative current change $100\% \cdot (I_2 - I_1)/I_1$ for each pair, and averaged the PPF/PPD index over 20 pairs. Three-frequency SRDP measurements were performed by applying fixed voltage pulses at three different frequencies: 1, 2.5, and 4 kHz, keeping the duration of the pulse trains the same (i.e., making number of pulses in the train proportional to frequency). Frequency-dependent SRDP measurements in the framework of BCM theory were performed by applying pulse

trains of 100 pulses, to further calculate relative current change from the start to the end current values of the pulse train: $100\% (I_{\text{last}} - I_{\text{first}})/I_{\text{first}}$, where I_{first} and I_{last} were averaged values of the first and last 5 pulses from a pulse train.

Acknowledgement

This work was supported by the Ministry of Science and Higher Education of the Russian Federation (Agreement No. 075-15-2021-589). The authors gratefully acknowledge the Shared Research Facilities Center of Moscow Institute of Physics and Technology (SRF MIPT) for the access to the probe station and SEM. A.G.N. acknowledges the Russian Science Foundation (project No 22-13-00436) for the synthesis of carbon nanotubes. The authors acknowledge the ITMO-MIPT-Skoltech Clover Program.

Supporting Information Available

References

- (1) Christensen, D. V.; Dittmann, R.; Linares-Barranco, B.; Sebastian, A.; Le Gallo, M.; Redaelli, A.; Slesazek, S.; Mikolajick, T.; Spiga, S.; Menzel, S.; others 2022 roadmap on neuromorphic computing and engineering. *Neuromorphic Computing and Engineering* **2022**, *2*, 022501.
- (2) Conklin, A. A.; Kumar, S. Solving the big computing problems in the twenty-first century. *Nature Electronics* **2023**, *6*, 464–466.
- (3) Marković, D.; Mizrahi, A.; Querlioz, D.; Grollier, J. Physics for neuromorphic computing. *Nature Reviews Physics* **2020**, *2*, 499–510.
- (4) Song, M.-K.; Kang, J.-H.; Zhang, X.; Ji, W.; Ascoli, A.; Messaris, I.; Demirkol, A. S.;

- Dong, B.; Aggarwal, S.; Wan, W.; others Recent advances and future prospects for memristive materials, devices, and systems. *ACS nano* **2023**, *17*, 11994–12039.
- (5) Ielmini, D.; Wang, Z.; Liu, Y. Brain-inspired computing via memory device physics. *APL Materials* **2021**, *9*.
- (6) Lynn, C. W.; Bassett, D. S. The physics of brain network structure, function and control. *Nature Reviews Physics* **2019**, *1*, 318–332.
- (7) Chaurasiya, R.; Shih, L.-C.; Chen, K.-T.; Chen, J.-S. Emerging higher-order memristors for bio-realistic neuromorphic computing: A review. *Materials Today* **2023**,
- (8) Kumar, S.; Wang, X.; Strachan, J. P.; Yang, Y.; Lu, W. D. Dynamical memristors for higher-complexity neuromorphic computing. *Nature Reviews Materials* **2022**, *7*, 575–591.
- (9) Kumar, S.; Williams, R. S.; Wang, Z. Third-order nanocircuit elements for neuromorphic engineering. *Nature* **2020**, *585*, 518–523.
- (10) Chua, L. O.; Kang, S. M. Memristive devices and systems. *Proceedings of the IEEE* **1976**, *64*, 209–223.
- (11) Bisquert, J. Device physics recipe to make spiking neurons. *Chemical Physics Reviews* **2023**, *4*.
- (12) Mikheev, V.; Chouprik, A.; Lebedinskii, Y.; Zarubin, S.; Matveyev, Y.; Kondratyuk, E.; Kozodaev, M. G.; Markeev, A. M.; Zenkevich, A.; Negrov, D. Ferroelectric second-order memristor. *ACS applied materials & interfaces* **2019**, *11*, 32108–32114.
- (13) Khanas, A.; Hebert, C.; Becerra, L.; Portier, X.; Jedrecy, N. Second-Order Memristor Based on All-Oxide Multiferroic Tunnel Junction for Biorealistic Emulation of Synapses. *Advanced Electronic Materials* **2022**, *8*, 2200421.

- (14) Cooper, L. N.; Bear, M. F. The BCM theory of synapse modification at 30: interaction of theory with experiment. *Nature Reviews Neuroscience* **2012**, *13*, 798–810.
- (15) Rittenhouse, C. D.; Shouval, H. Z.; Paradiso, M. A.; Bear, M. F. Monocular deprivation induces homosynaptic long-term depression in visual cortex. *Nature* **1999**, *397*, 347–350.
- (16) Frenkel, M. Y.; Bear, M. F. How monocular deprivation shifts ocular dominance in visual cortex of young mice. *Neuron* **2004**, *44*, 917–923.
- (17) Coleman, J. E.; Nahmani, M.; Gavornik, J. P.; Haslinger, R.; Heynen, A. J.; Erisir, A.; Bear, M. F. Rapid structural remodeling of thalamocortical synapses parallels experience-dependent functional plasticity in mouse primary visual cortex. *Journal of Neuroscience* **2010**, *30*, 9670–9682.
- (18) Wang, Z.; Zeng, T.; Ren, Y.; Lin, Y.; Xu, H.; Zhao, X.; Liu, Y.; Ielmini, D. Toward a generalized Bienenstock-Cooper-Munro rule for spatiotemporal learning via triplet-STDP in memristive devices. *Nature communications* **2020**, *11*, 1510.
- (19) John, R. A.; Milozzi, A.; Tsarev, S.; Brönnimann, R.; Boehme, S. C.; Wu, E.; Shorubalko, I.; Kovalenko, M. V.; Ielmini, D. Ionic-electronic halide perovskite memdiodes enabling neuromorphic computing with a second-order complexity. *Science Advances* **2022**, *8*, eade0072.
- (20) Jiang, C.; Liu, J.; Ni, Y.; Qu, S.; Liu, L.; Li, Y.; Yang, L.; Xu, W. Mammalian-brain-inspired neuromorphic motion-cognition nerve achieves cross-modal perceptual enhancement. *Nature Communications* **2023**, *14*, 1344.
- (21) Milano, G.; Pedretti, G.; Montano, K.; Ricci, S.; Hashemkhani, S.; Boarino, L.; Ielmini, D.; Ricciardi, C. In materia reservoir computing with a fully memristive architecture based on self-organizing nanowire networks. *Nature materials* **2022**, *21*, 195–202.

- (22) Zhang, Z.; Zhao, X.; Zhang, X.; Hou, X.; Ma, X.; Tang, S.; Zhang, Y.; Xu, G.; Liu, Q.; Long, S. In-sensor reservoir computing system for latent fingerprint recognition with deep ultraviolet photo-synapses and memristor array. *Nature Communications* **2022**, *13*, 6590.
- (23) Marunchenko, A. A.; Baranov, M. A.; Ushakova, E. V.; Ryabov, D. R.; Pushkarev, A. P.; Gets, D. S.; Nasibulin, A. G.; Makarov, S. V. Single-Walled Carbon Nanotube Thin Film for Flexible and Highly Responsive Perovskite Photodetector. *Advanced Functional Materials* **2022**, *32*, 2109834.
- (24) Noel, N. K.; Stranks, S. D.; Abate, A.; Wehrenfennig, C.; Guarnera, S.; Haghighirad, A.-A.; Sadhanala, A.; Eperon, G. E.; Pathak, S. K.; Johnston, M. B.; others Lead-free organic–inorganic tin halide perovskites for photovoltaic applications. *Energy & Environmental Science* **2014**, *7*, 3061–3068.
- (25) Stranks, S. D.; Snaith, H. J. Metal-halide perovskites for photovoltaic and light-emitting devices. *Nature nanotechnology* **2015**, *10*, 391–402.
- (26) John, R. A.; Demirağ, Y.; Shynkarenko, Y.; Berezovska, Y.; Ohannessian, N.; Payvand, M.; Zeng, P.; Bodnarchuk, M. I.; Krumeich, F.; Kara, G.; others Reconfigurable halide perovskite nanocrystal memristors for neuromorphic computing. *Nature communications* **2022**, *13*, 2074.
- (27) John, R. A.; Shah, N.; Vishwanath, S. K.; Ng, S. E.; Febriansyah, B.; Jagadeeswararao, M.; Chang, C.-H.; Basu, A.; Mathews, N. Halide perovskite memristors as flexible and reconfigurable physical unclonable functions. *Nature Communications* **2021**, *12*, 3681.
- (28) Park, Y.; Lee, J.-S. Metal halide perovskite-based memristors for emerging memory applications. *The Journal of Physical Chemistry Letters* **2022**, *13*, 5638–5647.

- (29) Marunchenko, A.; Kondratiev, V.; Pushkarev, A.; Khubezhov, S.; Baranov, M.; Nasibulin, A.; Makarov, S. Mixed Ionic-Electronic Conduction Enables Halide-Perovskite Electroluminescent Photodetector. *Laser & Photonics Reviews* **2023**, *17*, 2300141.
- (30) Sakhatskyi, K.; John, R. A.; Guerrero, A.; Tsarev, S.; Sabisch, S.; Das, T.; Matt, G. J.; Yakunin, S.; Cherniukh, I.; Kotyrba, M.; others Assessing the drawbacks and benefits of ion migration in lead halide perovskites. *ACS Energy Letters* **2022**, *7*, 3401–3414.
- (31) Zhumekenov, A. A.; Saidaminov, M. I.; Haque, M. A.; Alarousu, E.; Sarmah, S. P.; Murali, B.; Dursun, I.; Miao, X.-H.; Abdelhady, A. L.; Wu, T.; others Formamidinium lead halide perovskite crystals with unprecedented long carrier dynamics and diffusion length. *ACS Energy Letters* **2016**, *1*, 32–37.
- (32) Li, S.; Zhang, C.; Song, J.-J.; Xie, X.; Meng, J.-Q.; Xu, S. Metal halide perovskite single crystals: from growth process to application. *Crystals* **2018**, *8*, 220.
- (33) Feng, J.; Gong, C.; Gao, H.; Wen, W.; Gong, Y.; Jiang, X.; Zhang, B.; Wu, Y.; Wu, Y.; Fu, H.; others Single-crystalline layered metal-halide perovskite nanowires for ultrasensitive photodetectors. *Nature Electronics* **2018**, *1*, 404–410.
- (34) Xia, C. Q.; Peng, J.; Poncé, S.; Patel, J. B.; Wright, A. D.; Crothers, T. W.; Uller Rothmann, M.; Borchert, J.; Milot, R. L.; Kraus, H.; others Limits to electrical mobility in lead-halide perovskite semiconductors. *The journal of physical chemistry letters* **2021**, *12*, 3607–3617.
- (35) Zhang, D.; Zhang, Q.; Ren, B.; Zhu, Y.; Abdellah, M.; Fu, Y.; Cao, B.; Wang, C.; Gu, L.; Ding, Y.; others Large-scale planar and spherical light-emitting diodes based on arrays of perovskite quantum wires. *Nature Photonics* **2022**, *16*, 284–290.
- (36) Yang, X.; Ma, L.; Li, L.; Luo, M.; Wang, X.; Gong, Q.; Lu, C.; Zhu, R. Towards micro-PeLED displays. *Nature Reviews Materials* **2023**, 1–13.

- (37) Zhang, D.; Zhu, Y.; Zhang, Q.; Ren, B.; Cao, B.; Li, Q.; Poddar, S.; Zhou, Y.; Qiu, X.; He, Z.; others Vertical heterogeneous integration of metal halide perovskite quantum-wires/nanowires for flexible narrowband photodetectors. *Nano Letters* **2022**, *22*, 3062–3070.
- (38) Gu, Z.; Zhang, Y.; Zhao, Y.; Xu, Q.; Song, Y. From planar structures to curved optoelectronic devices: The advances of halide perovskite arrays. *Matter* **2023**, *6*, 2666–2696.
- (39) Nasibulin, A. G.; Kaskela, A.; Mustonen, K.; Anisimov, A. S.; Ruiz, V.; Kivisto, S.; Rackauskas, S.; Timmermans, M. Y.; Pudas, M.; Aitchison, B.; others Multifunctional free-standing single-walled carbon nanotube films. *ACS nano* **2011**, *5*, 3214–3221.
- (40) Pushkarev, A. P.; Korolev, V. I.; Markina, D. I.; Komissarenko, F. E.; Naujokaitis, A.; Drabavicius, A.; Pakstas, V.; Franckevicius, M.; Khubezhov, S. A.; Sannikov, D. A.; others A few-minute synthesis of CsPbBr₃ nanolasers with a high quality factor by spraying at ambient conditions. *ACS applied materials & interfaces* **2018**, *11*, 1040–1048.
- (41) Tao, S.; Schmidt, I.; Brocks, G.; Jiang, J.; Tranca, I.; Meerholz, K.; Olthof, S. Absolute energy level positions in tin-and lead-based halide perovskites. *Nature communications* **2019**, *10*, 2560.
- (42) Shiraishi, M.; Ata, M. Work function of carbon nanotubes. *Carbon* **2001**, *39*, 1913–1917.
- (43) Stranks, S. D.; Eperon, G. E.; Grancini, G.; Menelaou, C.; Alcocer, M. J.; Leijtens, T.; Herz, L. M.; Petrozza, A.; Snaith, H. J. Electron-hole diffusion lengths exceeding 1 micrometer in an organometal trihalide perovskite absorber. *Science* **2013**, *342*, 341–344.

- (44) Dong, Q.; Fang, Y.; Shao, Y.; Mulligan, P.; Qiu, J.; Cao, L.; Huang, J. Electron-hole diffusion lengths $> 175 \mu\text{m}$ in solution-grown $\text{CH}_3\text{NH}_3\text{PbI}_3$ single crystals. *Science* **2015**, *347*, 967–970.
- (45) Oksenberg, E.; Fai, C.; Scheblykin, I. G.; Joselevich, E.; Unger, E. L.; Unold, T.; Hages, C.; Merdasa, A. Deconvoluting energy transport mechanisms in metal halide perovskites using CsPbBr_3 nanowires as a model system. *Advanced functional materials* **2021**, *31*, 2010704.
- (46) Bisquert, J.; Guerrero, A.; Gonzales, C. Theory of hysteresis in halide perovskites by integration of the equivalent circuit. *ACS Physical Chemistry Au* **2021**, *1*, 25–44.
- (47) Yen, M.-C.; Lee, C.-J.; Liu, K.-H.; Peng, Y.; Leng, J.; Chang, T.-H.; Chang, C.-C.; Tamada, K.; Lee, Y.-J. All-inorganic perovskite quantum dot light-emitting memories. *Nature communications* **2021**, *12*, 4460.
- (48) Ravishankar, S.; Almora, O.; Echeverría-Arrondo, C.; Ghahremanirad, E.; Aranda, C.; Guerrero, A.; Fabregat-Santiago, F.; Zaban, A.; Garcia-Belmonte, G.; Bisquert, J. Surface polarization model for the dynamic hysteresis of perovskite solar cells. *The journal of physical chemistry letters* **2017**, *8*, 915–921.
- (49) Munoz-Diaz, L.; Rosa, A. J.; Bou, A.; Sánchez, R. S.; Romero, B.; John, R. A.; Kovalenko, M. V.; Guerrero, A.; Bisquert, J. Inductive and capacitive hysteresis of halide perovskite solar cells and memristors under illumination. *Frontiers in Energy Research* **2022**, *10*, 914115.
- (50) Tress, W.; Marinova, N.; Moehl, T.; Zakeeruddin, S. M.; Nazeeruddin, M. K.; Grätzel, M. Understanding the rate-dependent J–V hysteresis, slow time component, and aging in $\text{CH}_3\text{NH}_3\text{PbI}_3$ perovskite solar cells: the role of a compensated electric field. *Energy & Environmental Science* **2015**, *8*, 995–1004.

- (51) Liu, P.; Wang, W.; Liu, S.; Yang, H.; Shao, Z. Fundamental understanding of photocurrent hysteresis in perovskite solar cells. *Advanced Energy Materials* **2019**, *9*, 1803017.
- (52) Berruet, M.; Pérez-Martínez, J. C.; Romero, B.; Gonzales, C.; Al-Mayouf, A. M.; Guerrero, A.; Bisquert, J. Physical model for the current–voltage hysteresis and impedance of halide perovskite memristors. *ACS Energy Letters* **2022**, *7*, 1214–1222.
- (53) Rong, Y.; Hu, Y.; Ravishankar, S.; Liu, H.; Hou, X.; Sheng, Y.; Mei, A.; Wang, Q.; Li, D.; Xu, M.; others Tunable hysteresis effect for perovskite solar cells. *Energy & Environmental Science* **2017**, *10*, 2383–2391.
- (54) Gonzales, C.; Guerrero, A.; Bisquert, J. Transition from capacitive to inductive hysteresis: A neuron-style model to correlate I–V curves to impedances of metal halide perovskites. *The Journal of Physical Chemistry C* **2022**, *126*, 13560–13578.
- (55) Bisquert, J.; Gonzales, C.; Guerrero, A. Transient On/Off Photocurrent Response of Halide Perovskite Photodetectors. *The Journal of Physical Chemistry C* **2023**,
- (56) Augustine, G. J.; Eckert, R. Divalent cations differentially support transmitter release at the squid giant synapse. *The Journal of Physiology* **1984**, *346*, 257–271.
- (57) Chua, L.; Sirakoulis, G. C.; Adamatzky, A. *Handbook of Memristor Networks*; Springer Nature, 2019.
- (58) Bisquert, J.; Bou, A.; Guerrero, A.; Hernández-Balaguera, E. Resistance transient dynamics in switchable perovskite memristors. *APL Machine Learning* **2023**, *1*.
- (59) Peng, W.; Aranda, C.; Bakr, O. M.; Garcia-Belmonte, G.; Bisquert, J.; Guerrero, A. Quantification of ionic diffusion in lead halide perovskite single crystals. *ACS Energy Letters* **2018**, *3*, 1477–1481.
- (60) Guerrero, A.; Bisquert, J.; Garcia-Belmonte, G. Impedance spectroscopy of metal halide

- perovskite solar cells from the perspective of equivalent circuits. *Chemical Reviews* **2021**, *121*, 14430–14484.
- (61) Filipoiu, N.; Preda, A. T.; Anghel, D.-V.; Patru, R.; Brophy, R. E.; Kateb, M.; Besleaga, C.; Tomulescu, A. G.; Pintilie, I.; Manolescu, A.; others Capacitive and inductive effects in perovskite solar cells: the different roles of ionic current and ionic charge accumulation. *Physical Review Applied* **2022**, *18*, 064087.
- (62) Bisquert, J.; Guerrero, A. Chemical inductor. *Journal of the American Chemical Society* **2022**, *144*, 5996–6009.
- (63) Tung, R. T. The physics and chemistry of the Schottky barrier height. *Applied Physics Reviews* **2014**, *1*.
- (64) Juarez-Perez, E. J.; Sanchez, R. S.; Badia, L.; Garcia-Belmonte, G.; Kang, Y. S.; Mora-Sero, I.; Bisquert, J. Photoinduced giant dielectric constant in lead halide perovskite solar cells. *The journal of physical chemistry letters* **2014**, *5*, 2390–2394.
- (65) Zarazua, I.; Bisquert, J.; Garcia-Belmonte, G. Light-induced space-charge accumulation zone as photovoltaic mechanism in perovskite solar cells. *The journal of physical chemistry letters* **2016**, *7*, 525–528.
- (66) Guerrero, A.; Garcia-Belmonte, G.; Mora-Sero, I.; Bisquert, J.; Kang, Y. S.; Jacobsson, T. J.; Correa-Baena, J.-P.; Hagfeldt, A. Properties of contact and bulk impedances in hybrid lead halide perovskite solar cells including inductive loop elements. *The Journal of Physical Chemistry C* **2016**, *120*, 8023–8032.
- (67) Wang, Z.; Joshi, S.; Savel'ev, S. E.; Jiang, H.; Midya, R.; Lin, P.; Hu, M.; Ge, N.; Strachan, J. P.; Li, Z.; others Memristors with diffusive dynamics as synaptic emulators for neuromorphic computing. *Nature materials* **2017**, *16*, 101–108.

- (68) Milano, G.; Luebben, M.; Ma, Z.; Dunin-Borkowski, R.; Boarino, L.; Pirri, C. F.; Waser, R.; Ricciardi, C.; Valov, I. Self-limited single nanowire systems combining all-in-one memristive and neuromorphic functionalities. *Nature communications* **2018**, *9*, 5151.
- (69) Bienenstock, E. L.; Cooper, L. N.; Munro, P. W. Theory for the development of neuron selectivity: orientation specificity and binocular interaction in visual cortex. *Journal of Neuroscience* **1982**, *2*, 32–48.
- (70) Huang, Y.; Liu, J.; Harkin, J.; McDaid, L.; Luo, Y. An memristor-based synapse implementation using BCM learning rule. *Neurocomputing* **2021**, *423*, 336–342.
- (71) Marunchenko, A.; Kondratiev, V.; Pushkarev, A.; Khubezhov, S.; Baranov, M.; Nasibulin, A.; Makarov, S. Mixed Ionic-Electronic Conduction Enables Halide-Perovskite Electroluminescent Photodetector. *Laser & Photonics Reviews* 2300141.
- (72) Khabushev, E. M.; Krasnikov, D. V.; Zarembo, O. T.; Tsapenko, A. P.; Goldt, A. E.; Nasibulin, A. G. Machine learning for tailoring optoelectronic properties of single-walled carbon nanotube films. *The journal of physical chemistry letters* **2019**, *10*, 6962–6966.
- (73) Khabushev, E. M.; Krasnikov, D. V.; Kolodiaznaia, J. V.; Bubis, A. V.; Nasibulin, A. G. Structure-dependent performance of single-walled carbon nanotube films in transparent and conductive applications. *Carbon* **2020**, *161*, 712–717.
- (74) Kaskela, A.; Nasibulin, A. G.; Timmermans, M. Y.; Aitchison, B.; Papadimitratos, A.; Tian, Y.; Zhu, Z.; Jiang, H.; Brown, D. P.; Zakhidov, A.; others Aerosol-synthesized SWCNT networks with tunable conductivity and transparency by a dry transfer technique. *Nano letters* **2010**, *10*, 4349–4355.
- (75) Gilshteyn, E. P.; Romanov, S. A.; Kopylova, D. S.; Savostyanov, G. V.; Anisimov, A. S.; Glukhova, O. E.; Nasibulin, A. G. Mechanically tunable single-walled carbon nanotube

films as a universal material for transparent and stretchable electronics. *ACS applied materials & interfaces* **2019**, *11*, 27327–27334.

Supplementary material: Biorealistic Response in Optoelectrically-Driven Flexible Halide-Perovskite Single-Crystal Memristors

Ivan Matchenya,[†] Anton Khanas,[‡] Roman Podgorniy,[†] Daniil Shirkin,[†] Nikita Sizykh,[‡] Sergey Anoshkin,[†] Dmitry V. Krasnikov,[¶] Alexei Yulin,[†] Alexey Zhukov,[§] Albert G. Nasibulin,[¶] Ivan Scheblykin,^{||} Anatoly Pushkarev,^{*,†} Andrey Zenkevich,^{*,‡} and Alexandr Marunchenko^{*,†,||}

[†]*ITMO University, School of Physics and Engineering, St. Petersburg, 197101, Russian Federation*

[‡]*Moscow Institute of Physics and Technology (National research university), Institutskiy per. 9, Dolgoprudny, Moscow Region, 141701, Russia*

[¶]*Skolkovo Institute of Science and Technology, 30/1 Bolshoy Boulevard, 121205 Moscow, Russian Federation*

[§]*International Laboratory of Quantum Optoelectronics, HSE University, 190008, St. Petersburg, Russian Federation*

^{||}*Chemical Physics and NanoLund, Lund University, P.O. Box 124, 22100 Lund, Sweden*

E-mail: anatoly.pushkarev@metalab.ifmo.ru; zenkevich.av@mipt.ru;

a.marunchenko@metalab.ifmo.ru

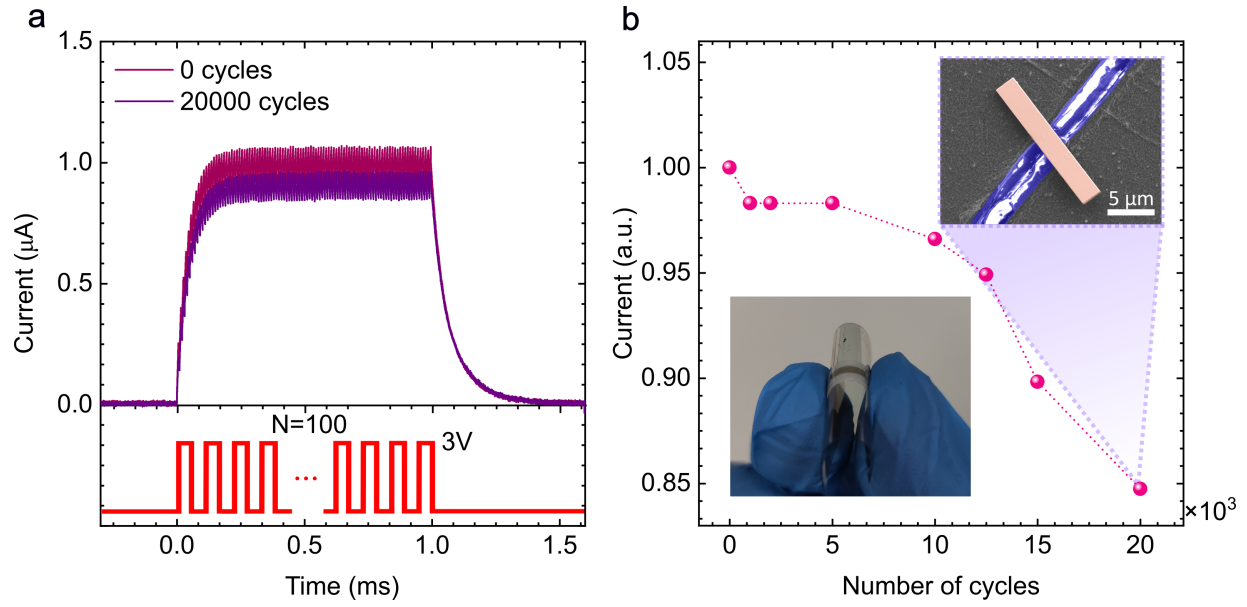


Figure S1: **Contact stability under optoelectronic stimuli combined with mechanical bending for 20000 cycles.** (a) Optoelectronic stimuli consist of 100 $5\mu\text{s}$ pulses at 3V and the repetition frequency of 150 kHz and 30 mW/cm^2 light illumination at a wavelength 470 nm. The normalized response of the device to this optoelectronic stimuli under mechanical bending of a tunable number of bending cycles is shown (b). The device response is measured after each 5000 bending cycle. The SEM image of the device after 20000 bending cycles, shows no visible changes in the morphology of the crystal (right inset image).

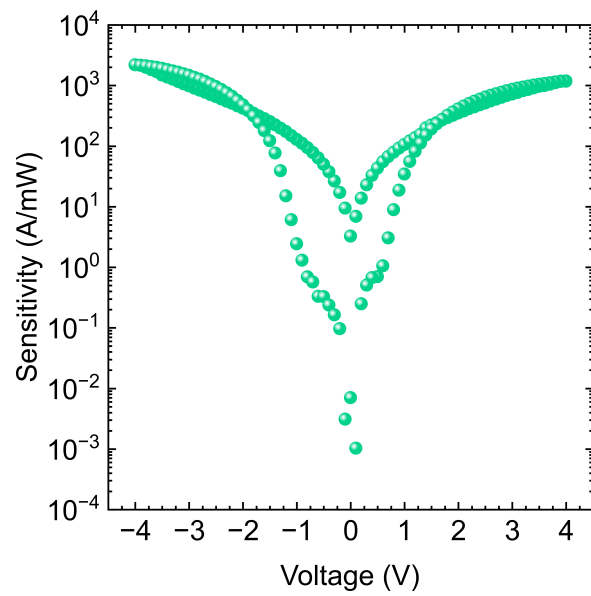


Figure S2: Voltage-dependent sensitivity of the photodetecting microcrystal.

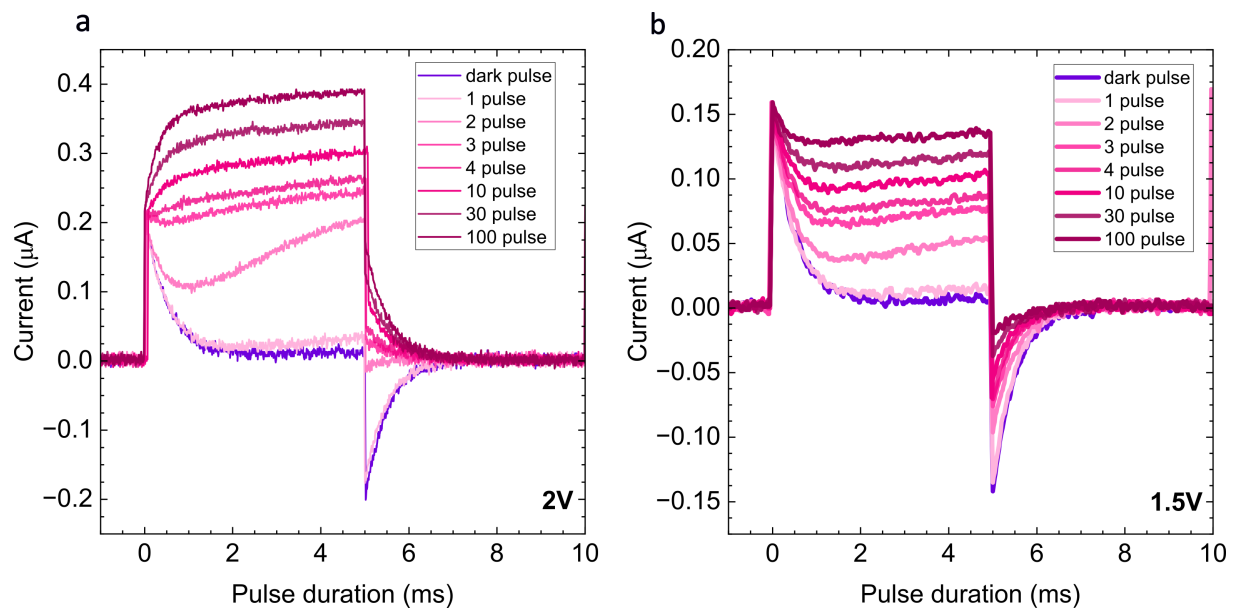


Figure S3: **Capacitance- and inductive-like transient kinetic under hybrid optoelectronic stimuli.** The electrical pulses with 5 ms pulse width at a 100 Hz repetition frequency and at 2V (3a), 1.5 V voltage magnitude (3b) are applied combined with the light at 30 mW/cm² intensity. The evolution of current flowing through a CsPbBr₃ microcrystal is shown at the 1st, 2nd, 3rd, 4th, 10th, 30th, and 100th pulses respectively. The dark corresponds to the first electrical pulse before the application of light stimuli.

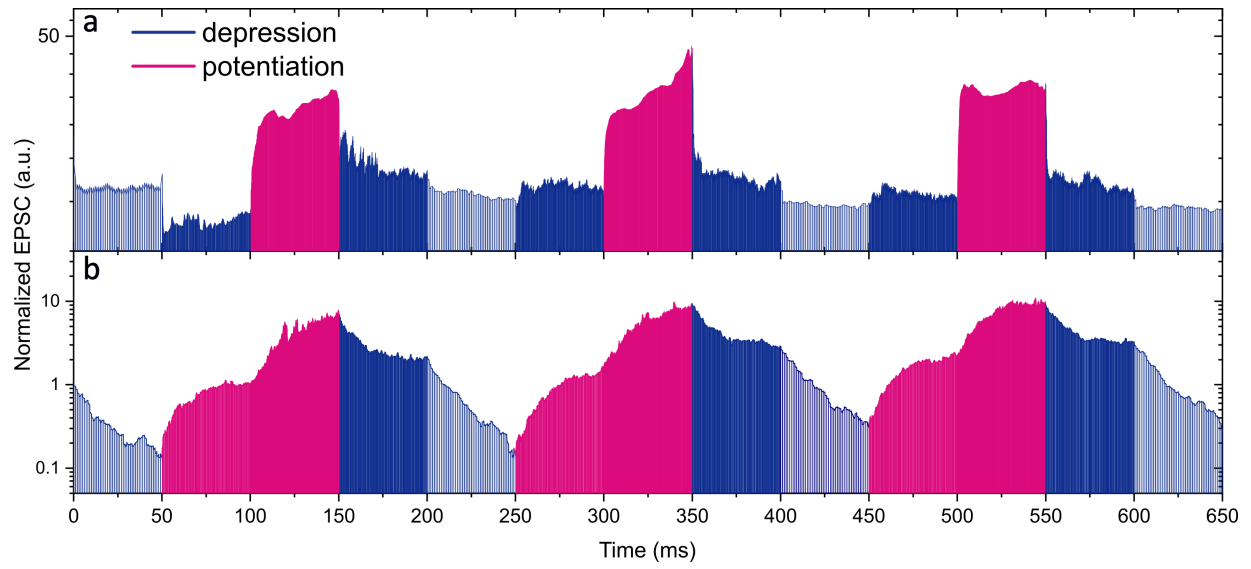


Figure S4: **Experience-dependent synaptic plasticity.** (a) SRDP measurements under light illumination (b) in the dark conditions.